

# Electrokinetic concentration enrichment within a microfluidic device using a hydrogel microplug†

Rahul Dhopeswarkar,<sup>b</sup> Li Sun<sup>a</sup> and Richard M. Crooks<sup>\*ab</sup>

Received 5th May 2005, Accepted 4th July 2005

First published as an Advance Article on the web 15th August 2005

DOI: 10.1039/b509063f

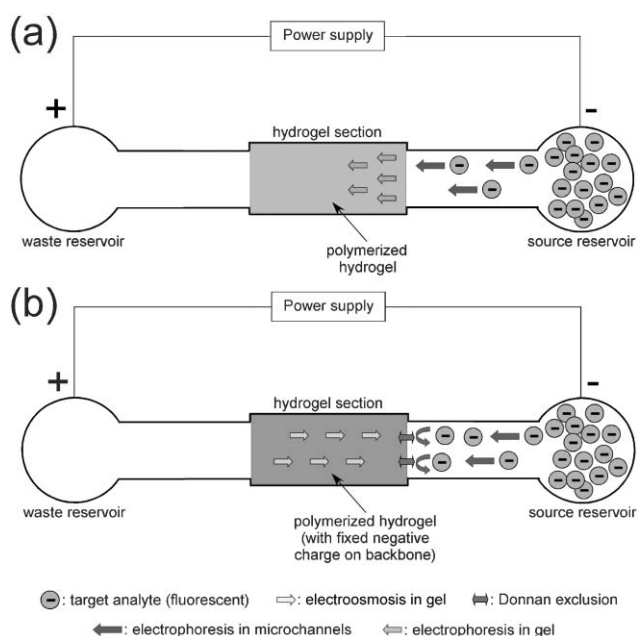
A simple and efficient approach for concentration of charged molecules in microfluidic devices is described. The functional component of the system is a hydrogel microplug photopolymerized within the main channel of a microfluidic device. When an appropriately biased voltage is applied across the hydrogel, charged analyte molecules move from the source well toward the hydrogel. Transport of the analyte through the hydrogel is slow compared to its velocity in the microfluidic channel, however, and therefore it concentrates at the hydrogel/solution interface. For an uncharged hydrogel, a bias of 100 V leads to a ~500-fold enrichment of the DNA concentration within 150 s, while the same conditions result in an enrichment of only 50-fold for fluorescein. Somewhat lower enrichment factors are observed when a negatively charged hydrogel is used. A qualitative model is proposed to account for the observed behavior.

## Introduction

Here we describe a new approach for concentrating charged molecules within a microfluidic device. The key finding is that a hydrogel microplug photopolymerized within the channel is able to modulate mass transport. The chemical composition of the hydrogel, including its charge and extent of crosslinking, determines the mechanism of concentration for a particular analyte. The trivial case occurs when the pore size of the hydrogel is smaller than the cross-sectional area of the analyte; then the hydrogel acts as a simple size-exclusion filter (we do not consider that case here).<sup>1,2</sup> If the pore size is slightly larger than the analyte, then the hydrogel exerts a dramatic effect on the electrophoretic velocity of the analyte (Part (a) of Scheme 1). If the hydrogel backbone bears fixed charges, then transport is affected by additional mechanisms including Donnan exclusion<sup>3–5</sup> and electroosmosis (Part (b) of Scheme 1).<sup>6</sup> We report findings for the concentration of negatively charged analytes (single-stranded DNA and fluorescein) using highly cross-linked neutral and anionic hydrogels. These materials can lead to analyte enrichment factors of ~500 in just 150 s. Moreover, the approach is simple and compatible with routine microfabrication techniques.

Microfluidic devices offer numerous advantages as chemical analysis platforms; among these is the ability to handle very small volumes of reagents. However, the correspondingly small number of molecules often results in a considerable loss

of detection sensitivity. The importance of lowering on-chip detection limits by concentrating the analyte is underscored by the large number of methods that have been developed to address this problem.<sup>7,8</sup> These include: field-amplified sample stacking (FASS),<sup>9–12</sup> solid-phase extraction (SPE),<sup>13–16</sup> isotachopheresis (ITP),<sup>17–19</sup> size-exclusion filtration,<sup>1,2</sup> electrokinetic micellar sweeping,<sup>20,21</sup> isoelectric focusing (IEF),<sup>22</sup> temperature-gradient focusing (TGF),<sup>23</sup> entropic trapping,<sup>24</sup> and evaporation.<sup>25</sup> However, a highly reproducible, and efficient (fast and with a high enrichment factor) concentration method with minimal microfabrication complexities has been elusive. For example, field-amplified sample stacking is one of the simplest enrichment methods and can achieve up to 1000-fold enrichment, but requires at least two buffer solutions and



Scheme 1

<sup>a</sup>Department of Chemistry, Texas A&M University, P. O. Box 30012, College Station, TX 77842-3012, USA

<sup>b</sup>Department of Chemical Engineering, Texas A&M University, Mailstop 3122, College Station, TX 77843-3122, USA.  
E-mail: crooks@tamu.edu; Fax: +1-979-845-1399; Tel: +1-979-845-5629

† Electronic supplementary information (ESI) available: Optical images of the microfabricated neutral and anionic hydrogel plugs after conditioning, fluorescence micrographs obtained during concentration of fluorescein, and movies (MPG format) showing the entire concentration experiments represented by Fig. 2, 4, 5 and 7 in the paper. See <http://dx.doi.org/10.1039/b509063f>

a relatively large amount of chip space. Solid-phase extraction techniques can yield concentration factors of  $>500$ , but they involve the complexity of incorporating appropriate capture and release chemistries inside a microchannel. TGF is capable of achieving extremely high enrichment factors ( $>10,000$  in 40 min), but it requires special buffers, a high operating voltage ( $\sim 1000$  V), and precise temperature control.

The results described here are an extension of a previous study in which we showed that a nanoporous polyester membrane could be used to concentrate DNA in a three-dimensional microfluidic architecture.<sup>6</sup> Specifically, the results of this earlier study showed that in the absence of similitude,<sup>26</sup> it was possible to achieve a balance between the electrophoretic velocity of a charged analyte and the electroosmotic velocity of the solvent. This resulted in a net zero velocity of the analyte near the nanoporous membrane. However, we abandoned this analyte-concentration approach, because it was difficult to reproducibly seal the 10  $\mu\text{m}$  thick nanoporous membrane between the two fluidic channels. The insight that led to the present findings is that the pores within a track-etched polymeric membrane are similar in some important ways to those found within a hydrogel. This means that the same type of concentration effect we observed in the more complicated three-dimensional system is exhibited by a simple, two-dimensional microfluidic device incorporating a microfabricated hydrogel plug. In addition to simplifying the fabrication process, the hydrogel microplug approach provides more design flexibility.

There have been a number of previous studies focusing on the integration of hydrogels into microfluidic devices. For example, pH-responsive hydrogels have been used as microfluidic valves by Beebe, Moore, and coworkers.<sup>27–29</sup> Likewise, poly(ethylene glycol)-based hydrogel microstructures have been shown to function as passive switches in DNA hybridization arrays.<sup>30</sup> Cells, such as *E. coli*, have been immobilized within hydrogels and used as sensors.<sup>31</sup> Finally, Tarlov and coworkers reported an interesting approach for label-free detection of DNA using hydrogel plugs in microfluidic channels.<sup>15,32,33</sup>

Here, we show that two different negatively charged analytes, single-stranded DNA (ssDNA) and fluorescein, can be concentrated using both neutral and anionic hydrogel transport modulators. Within 150 s the neutral hydrogel concentrates ssDNA and fluorescein by factors of 500 and 50, respectively. The corresponding enrichment factors for the anionic hydrogel are 240 and 15, respectively. Although this approach is not optimized, these enrichment factors are comparable to those obtained using most of the more experimentally challenging methods for concentrating analytes mentioned previously. We interpret the results of this study in terms of a qualitative hypothesis. A quantitative analysis, which is presently underway, awaits accurate experimental measurements of some difficult-to-determine electrokinetic parameters and then validation of the hypothesis using appropriate fluid-dynamics simulations.

## Experimental

### Chemicals

Precursors for preparing poly(dimethylsiloxane) (PDMS, Sylgard 184) microfluidic devices were obtained from

Krayden, Inc. (Denver, CO). Fluorescein disodium salt (98+%, Avocado, Heysham, England), 5'-fluorescein-labeled ssDNA (a 22-mer, IDT, Coralville, IA), TRIS base and its hydrochloride salt (TRIZMA brand), acrylic acid (AA), 2-hydroxyethyl methacrylate (HEMA), ethylene glycol dimethacrylate (EGDM), and Irgacure 651 (Sigma-Aldrich, St. Louis, MO) were used as received. All buffer solutions contained 5.0 mM TRIS and 5.0 mM TRIS·HCl (pH 8.3) and were prepared with deionized water (18 M $\Omega$  cm, Milli-Q, Millipore).

### Device fabrication and layout

Microfluidic channels (20–25  $\mu\text{m}$  in height) were fabricated following a literature procedure.<sup>34</sup> The PDMS monolith (about 6 mm thick) containing the channel was bonded irreversibly to a cover glass (24 mm  $\times$  24 mm, 0.13–0.17 mm thick, VWR Scientific) after both were treated with an O<sub>2</sub> plasma (60 W, model PDC-32G, Harrick Scientific, Ossining, NY) for 30 s. The layout of the channels in the resulting device is shown in Fig. 1. The primary microchannel is 90–100  $\mu\text{m}$  wide and 7–7.5 mm long. A wider section of channel (190–200  $\mu\text{m}$  wide and 400  $\mu\text{m}$  long) designed to house the hydrogel microplug is located in the middle of the primary microchannel. The primary microchannel terminates in two 3 mm diameter reservoirs (ResA and ResB), and it intersects side channels SCh-A and SCh-B. The latter terminate in reservoirs A' and B' (ResA' and ResB'). ResA' and ResB' are necessary to remove the hydrogel precursor from the primary channel following photopolymerization. Two slightly different device

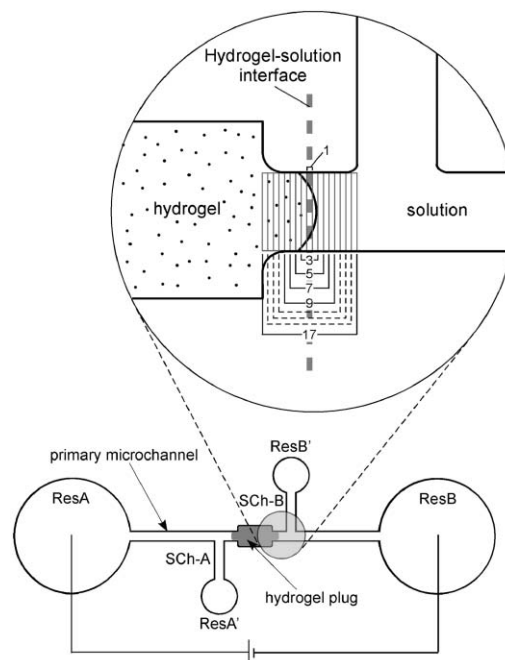


**Fig. 1** Schematic illustration of the microfluidic device used for concentration of ssDNA. The enlarged view shows how the channel cross-sections were defined for quantifying the enrichment factors. A region of interest (ROI) of 1 pixel width (smallest possible area at the selected resolution) was chosen to be as close as possible to the hydrogel/solution interface and other ROIs of increasing widths (denoted by the corresponding numerical values in the enlarged view) were also centered at the hydrogel/solution interface.

designs were used for these studies. The design shown in Fig. 1, in which the angle between the primary and secondary channels is 90°, was used for DNA concentration, and another design (see Fig. S2 in the Electronic supplementary information (ESI)†) having the side channels at 45° relative to the main channel, was used for the fluorescein concentration experiments. This aspect of the device design resulted from an attempt to optimize the side channel configuration, but in fact, the performance arising from both designs was indistinguishable.

### Hydrogel microplug fabrication

The hydrogel microplugs were fabricated as follows. First, a hydrogel precursor solution was introduced into the primary microchannel by capillary action. Second, UV light (365 nm, 200 s, 300 mW cm<sup>-2</sup>, EFOS Lite E3000, Ontario, Canada) was projected onto the wide part of the central channel from the side port of a microscope (DIAPHOT 300, Nikon) through a 10× objective lens. Unpolymerized precursor solution was removed by pumping 10.0 mM TRIS buffer (pH = 8.3) through the primary and secondary channels at a flow rate of 10.0 μL min<sup>-1</sup> for >10 min using a syringe pump (Harvard Apparatus, Holliston, MA).

### Procedures and data analysis

The electric field inside the primary microchannel was introduced by applying a bias voltage between two coil electrodes (90% Pt/10% Ir, 0.25 mm in diameter and 50.0 mm in length) immersed in ResA and ResB. The bias voltage (range 0–1067 V, Ultra Volt, Ronkonkoma, NY) could be switched with a time resolution of 100 ms using a computer and custom software. Before each experiment, the primary microchannel was filled with 10.0 mM TRIS buffer (pH 8.3), and then the hydrogel microplug was conditioned by applying a 100–300 V bias. The conditioning step removes unpolymerized precursor solution from within the hydrogel. After conditioning, 10.0 mM TRIS buffer was pumped into the left side of the microfluidic system (Fig. 1) from ResA'. In addition, 10.0 mM TRIS buffer containing the fluorescent analyte (5.0 μM fluorescein or 5.0 μM fluorescein-labeled DNA) was pumped into the right side from ResB' and also into an isolated reference channel for calibration purposes. The syringe pump was disconnected after ensuring that the solutions in all the reservoirs were at approximately the same height (to eliminate pressure-driven flow within the channels). Finally, a programmed sequence of bias voltages (Table 1) was applied to the electrodes, and simultaneously a set of fluorescence micrographs was obtained from the region near

**Table 1** Programmed switching of the bias voltage between Reservoirs A and B (ResA and ResB, Fig. 1)

Time/s	Program action
<0	0 V bias
0	100 V forward bias (ResA positive)
150	0 V bias
170	100 V reverse bias (ResB positive)
320	0 V bias

the hydrogel/open-channel interface (V++ software, Digital Optics, New Zealand, 1 frame s<sup>-1</sup>) using an inverted microscope (TE 300, Nikon, Japan) equipped with a CCD camera (SenSys 1410E, Photometrics, Tucson, AZ). Typically, a total of 360 frames (8 × 8 binning, or 163 × 128 pixels) were captured through a 4× objective lens.

To quantify the enrichment factor near the hydrogel/solution interface, the average fluorescence intensity (counts per second per pixel) was calculated by first integrating the fluorescence over a particular region of interest (ROI) and then dividing the result by the total number of pixels in the ROI. The same calculation was also performed over a second ROI located within the reference channel. The enhancement factor is the ratio of the two fluorescence intensities obtained according to the above procedure. Because the fluorescence intensity has a non-uniform distribution, successively larger ROIs were chosen to calculate the enrichment factors. The inset of Fig. 1 shows that the smallest ROI has a width of 1 pixel and is centered at the hydrogel/solution interface. Other ROIs having increasing widths (3, 5...17 pixels) are centered at this same location. All fluorescence intensity values were corrected by subtracting the background (dark count), which was obtained using a ROI outside the channel at *t* = 0 s. The effect of photobleaching was not corrected in any reported data. However, control experiments using fluorescein indicated that the decrease in fluorescence intensity due to photobleaching was less than 6% over a period of 400 s of illumination.

## Results and discussion

### Properties of the hydrogel microplugs

The hydrogels were photopolymerized as highly cross-linked microplugs within the primary channels of the microfluidic devices using projected UV light.<sup>29</sup> The anionic poly(HEMA-co-AA) hydrogel has a tendency to swell in basic buffers because of the negative charge on its backbone.<sup>4,28</sup> As depicted schematically in the inset of Fig. 1, this leads to a slight bulging of the hydrogel along the long axis of the primary channel. Less swelling was observed for the neutral hydrogel. This swelling is advantageous, because it helps to seal the microplug against the channel wall thereby preventing analyte transport through macroscopic leaks that might otherwise develop at these interfaces. Swelling also ensures that the hydrogel microplug remains stationary even under the influence of high electric fields and the pressure-driven flow used during device fabrication. Covalent attachment of the microplug to the walls of the primary channel was thus not required.<sup>35</sup>

The type of highly cross-linked HEMA hydrogel microplugs used in this study have a nanoporous structure with an average pore size of 1.6 nm to 1.9 nm.<sup>36</sup> This dimension can be compared to those estimated for the analytes: the 22-mer ssDNA (MW ~ 7.252 kDa) has a mean diameter of ~1.3 nm and a length of ~10 nm,<sup>37,38</sup> and fluorescein can be approximated as a disk having a diameter of ~0.7 nm.<sup>39</sup> The important point is that the analytes have a limiting dimension smaller than that of the hydrogel pore size. This makes it unlikely that concentration arises from simple size exclusion.

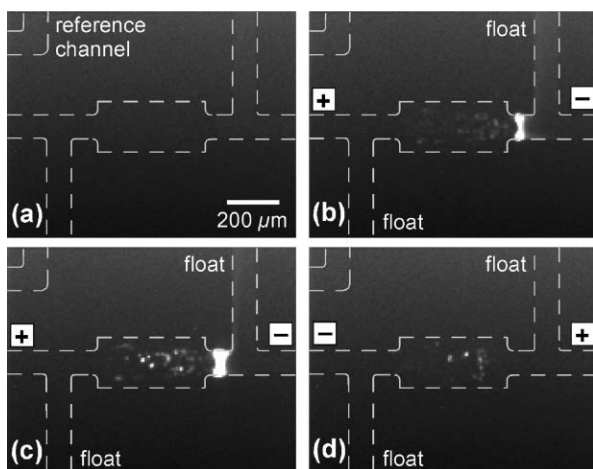


**Fig. 2** Fluorescence micrographs obtained during concentration of ssDNA using the neutral hydrogel in the microfluidic device layout shown in Fig. 1. (a) Before applying a potential bias. After applying a forward bias of 100 V for (b) 50 s and (c) 150 s. (d) 50 s after applying a reverse bias of 100 V (total elapsed time = 220 s). No bias voltage was applied to the side channels labeled “float”. The image size was 163 pixels  $\times$  128 pixels, and the full-scale intensity range was 160 to 4095 counts per pixel. The complete movie is provided in the ESI (Movie S1).

#### Analyte concentration using neutral hydrogel microplugs

Fig. 2 is a series of four fluorescence micrographs that demonstrate concentration of ssDNA by a neutral hydrogel microplug. The complete movie from which these individual frames were extracted is provided in the ESI. Note that the device layout incorporates an isolated reference channel, present in the upper-left corner of each micrograph, which contains a known concentration of fluorescently labeled DNA. This is used for calibration purposes.

The micrograph in Fig. 2(a) was obtained prior to the application of a bias voltage. Fig. 2(b) was obtained after applying a 100 V forward bias (ResA at positive potential, Table 1) for 50 s. During this time negatively charged DNA migrates from right to left, but the neutral hydrogel acts as a barrier that greatly reduces its electrophoretic velocity. This results in concentration of DNA near the hydrogel/solution interface. Indeed, an enrichment factor of  $\sim 500$  is achieved after 150 s (Fig. 2(c)). This micrograph also shows that some DNA moves into the hydrogel. When the bias voltage is reversed (Fig. 2(d)), DNA is rapidly transported away from the concentrated region and back toward ResB. However, some of the DNA trapped within the hydrogel remains.<sup>40</sup>

Fig. 3(a) shows how the enrichment factor varies as a function of the width of the region of interest (ROI, see Experimental Section and the inset of Fig. 1) over which the fluorescent signal is averaged. Data are provided prior to the experiment ( $t < 0$  s) and at three different times (50, 100, and 150 s) following application of the bias voltage. The maximum enrichment factor is obtained when the ROI has the minimum width (1 pixel). As the width of the ROI increases, the enrichment factor decreases. An ROI width of 3 pixels was selected for quantitative analysis, because these data were less subject to slight variations in the alignment of the microscope with the hydrogel-solution interface; that is, they were easily reproduced.

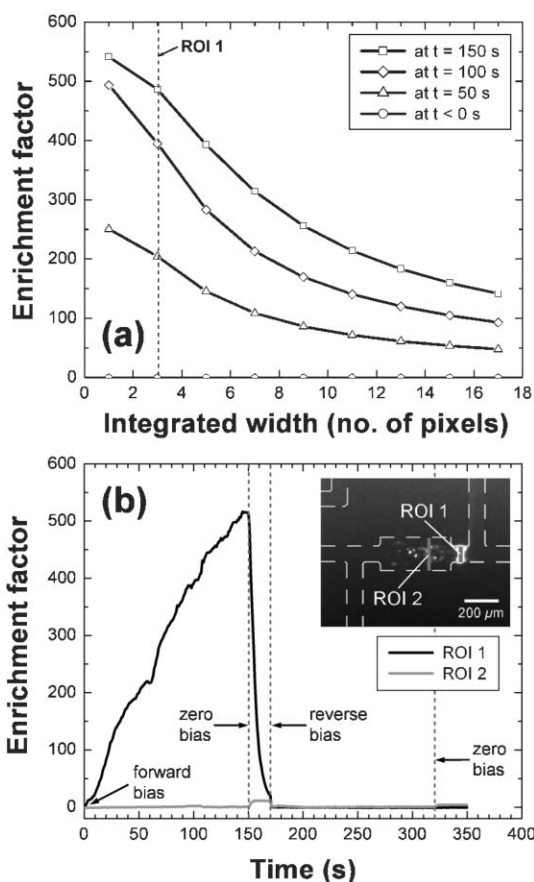


**Fig. 3** Data derived from the micrographs shown in Fig. 2 for concentration of ssDNA in the neutral hydrogel. (a) Enrichment factors calculated using ROIs having different pixel widths (see inset of Fig. 1). (b) Enrichment factor as a function of time for a 3 pixel-wide ROI centered at the hydrogel/solution interface (black solid line, ROI 1) and in the hydrogel interior (grey solid line, ROI 2). The grey areas indicated in the inset define the location of ROI 1 and ROI 2.

Fig. 3(b) is a plot of the enrichment factor near the hydrogel surface (ROI 1, which is 3 pixels wide and corresponds to the dashed line in Fig. 3(a)) as a function of time following application of a 100 V bias (black). The enrichment factor increased approximately linearly with time until 150 s when the bias was switched to 0 V. Under these conditions the concentration of the enriched DNA band gradually decreased because of steady loss of DNA through the side channel (see the movie provided in the ESI), and the enrichment factor decreased to  $\sim 21$  at  $t = 170$  s. The reason for leakage of the concentrated band through the side channel under these conditions is not clear at present. After 20 s at 0 V bias, a reverse bias of 100 V was applied and the remaining DNA was driven back to ResB. The enrichment factor as a function of time is also shown for ROI 2 inside the hydrogel (grey solid line). The amount of ssDNA that is able to penetrate the hydrogel interior is clearly insignificant compared to the amount concentrated at the hydrogel/solution interface.

Experiments similar to those described for DNA were carried out using fluorescein, which is a small dye molecule carrying two negative charges at the pH used for these experiments.<sup>41</sup> The results (four individual frames are shown in

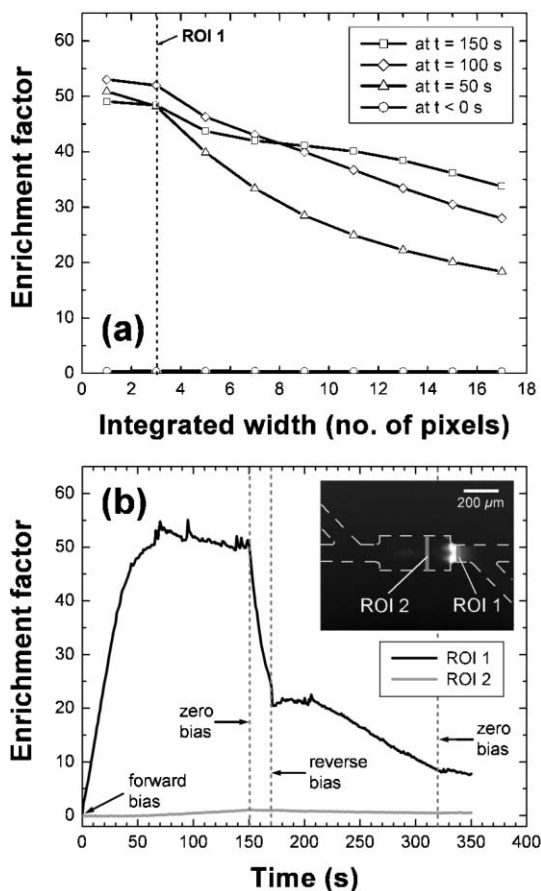


**Fig. 4** Data for the concentration of fluorescein in the neutral hydrogel derived from the micrographs shown in Fig. S3 using the device layout shown in Fig. S2 (see ESI). (a) Enrichment factors calculated using ROIs having different pixel widths (see the inset in Fig. 1). (b) Enrichment factor as a function of time for a 3 pixel-wide ROI centered at the hydrogel/solution interface (black, ROI 1) and in the hydrogel interior (solid grey line, ROI 2). The grey areas indicated in the inset defines the location of ROI 1 and ROI 2.

Fig. S3 and the complete movie is provided in the ESI) are qualitatively similar to those for DNA. However, as shown in Fig. 4(a), the initial enrichment factors are about an order of magnitude smaller than for DNA (50 vs. 500, respectively). Additionally, the enriched fluorescein band is much broader than for DNA (compare the rate at which the enrichment factor decreases as a function of the integrated pixel width in Fig. 3(a) and 4(a)). Fig. 4(b) shows that the maximum enrichment factor for fluorescein is achieved within 70 to 80 s, and that further application of the bias voltage actually results in a slight decrease. When the bias is switched to 0 V at  $t = 150$  s, the enriched fluorescein band disperses at a slower rate than ssDNA (compare Fig. 3(b)). When the bias is reversed at  $t = 170$  s, the fluorescence intensity in ROI 1 remains constant for about 40 s, and then decreases gradually. Recall that the concentration of ssDNA approached zero upon bias reversal (Fig. 3(b)). We interpret these results in terms of a greater extent of penetration of fluorescein into the hydrogel microplug during application of the forward bias, followed by slow release upon bias reversal.

Although we are not prepared to offer a quantitative explanation for the concentration results shown in Fig. 2–4, we have developed a simple qualitative model that accounts for the observations reported thus far. We believe that the highly cross-linked hydrogel matrix provides a resistance to ionic mass transfer. This of course increases the magnitude of the electric field inside the hydrogel microplug,<sup>42,43</sup> which should in turn increase the electrophoretic velocity of charged molecules within the microplug. However, the inhomogeneous nature of the hydrogel results in formation of dead ends and tortuous paths,<sup>5</sup> and therefore the resistance presented by the hydrogel is ion selective: smaller ions, such as those comprising the buffer, carry a higher percentage of the current in the hydrogel than they do in the open channel. Accordingly, the larger analytes carry a smaller percentage of the current in the hydrogel, and this results in their being concentrated at the hydrogel/solution interface. Another way of saying this is that the electrophoretic mobilities of the 22-mer ssDNA (MW  $\sim 7.252$  kDa) and fluorescein (MW  $\sim 0.376$  kDa) inside the hydrogel are much smaller than in the open channel. In contrast, the buffer ions are sufficiently small that their mobility is not as medium-dependent. This same argument accounts for the much higher enrichment factor for ssDNA compared to fluorescein. The situation is directly analogous to the differential mobility of different molecular weight DNA oligos observed in gel electrophoresis.

#### Concentration using anionic hydrogel microplugs

We thought it might be possible to eliminate analyte penetration into the hydrogel, and thus increase the enrichment factor, by using negatively charged microplugs. Accordingly, we co-polymerized acrylic acid and 2-hydroxyethyl methacrylate to introduce fixed negative charges onto the hydrogel backbone, and then carried out experiments identical to those described for the neutral hydrogel microplugs.

Fig. 5 is a series of four fluorescence micrographs obtained before and during application of a 100 V bias voltage to a solution containing 22-mer ssDNA. Prior to application of the bias voltage the fluorescence intensity of the DNA-containing solution is below the detection limit of the measurement system (Fig. 5(a)). However, when a 100 V forward bias is applied ssDNA begins to concentrate in the vicinity of hydrogel surface (Fig. 5(b) and (c)). An enrichment factor of  $\sim 240$  is obtained within 150 s. When the bias is reversed, the enriched DNA band moves rapidly back toward ResB (Fig. 5(d)). The complete movie from which the individual frames shown in Fig. 5 were extracted is provided in the ESI.

Fig. 6 provides an analysis of the concentration data for ssDNA that is analogous to that previously discussed for the neutral hydrogel. There are four important observations that can be made from the data in Fig. 5 and 6. First, concentration of DNA at ROI 1 increases linearly as a function of time until the bias is switched to 0 V, just as it did for the neutral hydrogel. Second, a maximum enrichment factor is not attained during the 150 s allotted for the experiment. Third, and most surprising, the enrichment factor is lower for the anionic hydrogel than for the analogous neutral gel. Fourth,

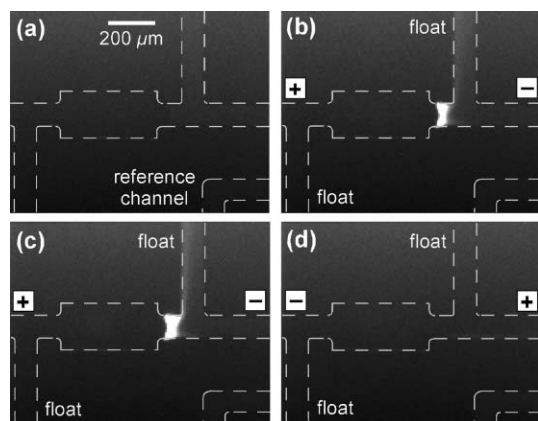


**Fig. 5** Fluorescence micrographs obtained during concentration of ssDNA using the anionic hydrogel in the microfluidic device layout shown in Fig. 1. (a) Before applying a potential bias. After applying a forward bias of 100 V for (b) 50 s and (c) 150 s. (d) 50 s after applying a reverse bias of 100 V (total elapsed time = 220 s). No bias voltage was applied to the side channels labeled “float”. The image size was 163 pixels  $\times$  128 pixels, and the full-scale intensity range was 154 to 4024 counts per pixel. The complete movie is provided in the ESI (Movie S3).

no DNA can be detected in the hydrogel interior during either the period of the forward or reverse bias.

Data for the concentration of fluorescein using the anionic hydrogel are shown in Fig. S4 (ESI) and Fig. 7. As for ssDNA, the maximum enrichment factor for fluorescein is substantially lower for the anionic hydrogel compared to the neutral gel: 15 vs. 50, respectively. Also, there is no detectable penetration of fluorescein into the anionic microplug. For the anionic hydrogel, a maximum steady-state enrichment factor for fluorescein is attained within about 100 s.

In addition to the ion-size-based differential resistance of the neutral hydrogel discussed earlier, the anionic hydrogel imposes two additional barriers to penetration by negatively charged ions. The first of these arises from Donnan exclusion.<sup>3–5</sup> Donnan exclusion is operative when the polymer backbone contains fixed charges and the size of the pores within the gel are smaller than the Debye length (that is, the double-layer thickness). Both of these conditions are met for the anionic hydrogels. For example, the average pore size is 1.6 to 1.9 nm,<sup>36</sup> and the calculated Debye length for a 10.0 mM 1:1 electrolyte solution is 3.0 nm.<sup>44</sup> Donnan exclusion ensures that the number of negatively charged analyte molecules will be greatly reduced in the hydrogel interior, and this prediction is in accord with the experimental observations shown in Fig. 5–7: both ssDNA and fluorescein are undetectable in the hydrogel interior.

The second difference between the neutral and charged hydrogels relates to the existence of electroosmotic flow (EOF) generated within the pores of the latter. Because the Debye length (3.0 nm) is larger than the average pore size (1.6 to 1.9 nm) the EOF velocity will be reduced,<sup>45,46</sup> but a careful examination of the data in Fig. 5 and Fig. S4 (see ESI) reveals that EOF still exerts a detectable effect on analyte transport. Specifically, there is clear visual evidence that EOF generated by the anionic hydrogel results in streaming of ssDNA and fluorescein from the analyte-enriched band near the

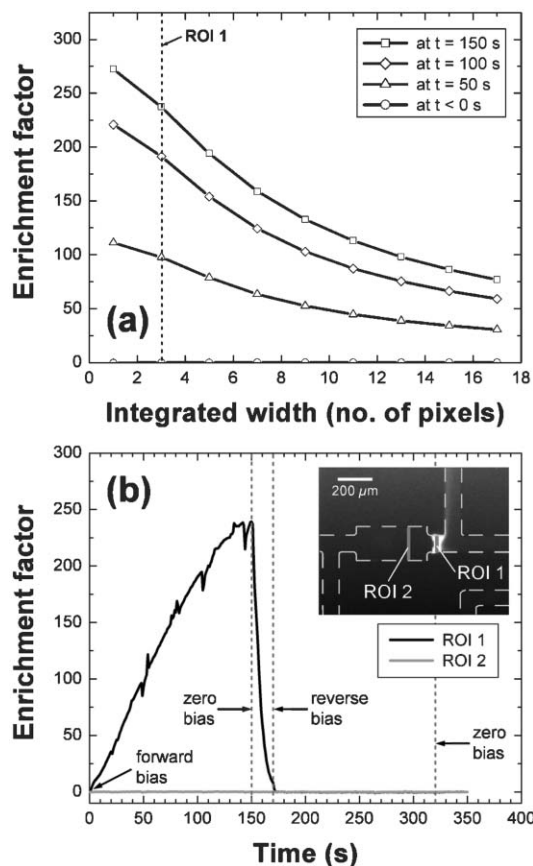


**Fig. 6** Data derived from the micrographs shown in Fig. 5 for concentration of ssDNA in the anionic hydrogel. (a) Enrichment factors calculated using ROIs having different pixel widths (see the inset in Fig. 1). (b) Enrichment factor as a function of time for a 3 pixel-wide ROI centered at the hydrogel/solution interface (black solid line, ROI 1) and in the hydrogel interior (grey solid line, ROI 2). The grey areas indicated in the inset define the location of ROI 1 and ROI 2.

gel/solution interface down the side channel leading to ResB'. We believe this phenomenon is responsible for the lower enrichment factor for the anionic hydrogel compared to the neutral hydrogel.<sup>42</sup>

## Summary and conclusions

We have demonstrated a new approach for electrokinetic concentration of charged analytes inside microfluidic channels containing a microfabricated hydrogel microplug. The approach is very simple and compatible with standard microfabrication methodologies. Concentration is most effective for large, highly charged molecules like DNA, and enrichment factors of 500 can be obtained within 150 s using low bias voltages (100 V). This method has not been optimized yet, but it seems likely that significantly higher enrichment factors will be obtainable when the system is better understood. Likewise, there is a clear incentive to devise a means for eliminating the side channels from the device layout, because in their absence the EOF may not limit the enrichment factors attainable using anionic hydrogel microplugs. Studies intended to address these experimental issues are presently underway. Simulation and

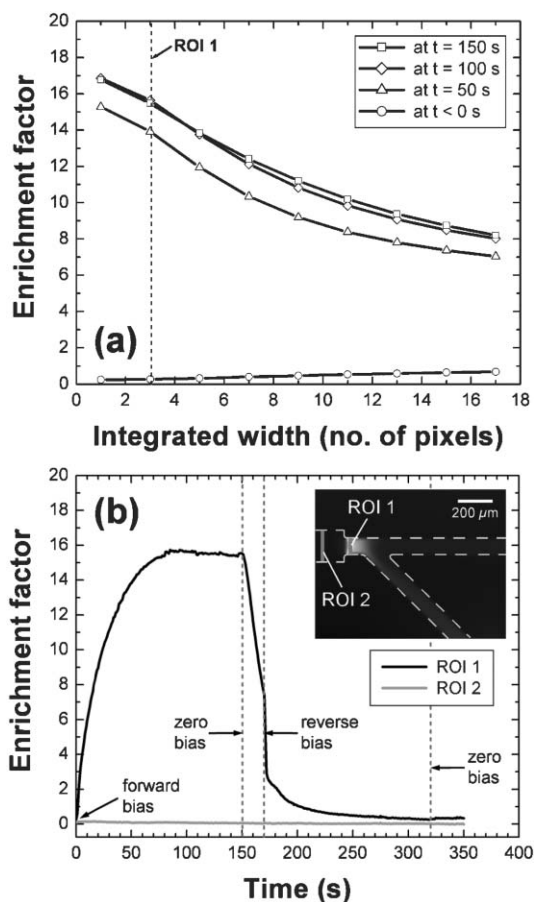


**Fig. 7** Data derived from the micrographs shown in Fig. S4 using the device layout shown in Fig. S2 (see ESI) for the concentration of fluorescein using the anionic hydrogel. (a) Enrichment factors calculated using ROIs having different pixel widths (see the inset in Fig. 1). (b) Enrichment factor as a function of time for a 3 pixel-wide ROI centered at the hydrogel/solution interface (black solid line, ROI 1) and in the hydrogel interior (grey solid line, ROI 2). The grey areas indicated in the inset define the location of ROI 1 and ROI 2.

modeling studies are also underway to develop a better theoretical understanding of the results presented herein. We envisage that when this concentration methodology is fully developed it will be useful for lowering the detection limit for a variety of on-chip bioassays.

## Acknowledgements

Full financial support for this work was provided by the US Department of Energy, Office of Basic Energy Sciences (Contract No. DE-FG02-01ER15247).

## References

- S. Song, A. K. Singh and B. J. Kirby, *Anal. Chem.*, 2004, **76**, 4589–4592.
- J. Khandurina, S. C. Jacobson, L. C. Waters, R. S. Foote and J. M. Ramsey, *Anal. Chem.*, 1999, **71**, 1815–1819.
- F. G. Donnan, *J. Membr. Sci.*, 1995, **100**, 45–55.
- N. A. Peppas and A. R. Khare, *Adv. Drug Delivery Rev.*, 1993, **11**, 1–35.
- A. S. Hoffman, *Adv. Drug Delivery Rev.*, 2002, **43**, 3–12.
- J. Dai, T. Ito, L. Sun and R. M. Crooks, *J. Am. Chem. Soc.*, 2003, **125**, 13026–13027.
- J. Lichtenberg, N. F. de Rooij and E. Verpoorte, *Talanta*, 2002, **56**, 233–266.
- G. J. M. Bruin, *Electrophoresis*, 2000, **21**, 3931–3951.
- R.-L. Chien, *Electrophoresis*, 2003, **24**, 486–497.
- B. Jung, R. Bharadwaj and J. G. Santiago, *Electrophoresis*, 2003, **24**, 3476–3483.
- J. Lichtenberg, E. Verpoorte and N. F. de Rooij, *Electrophoresis*, 2001, **22**, 258–271.
- R.-L. Chien and D. S. Burgi, *Anal. Chem.*, 1992, **64**, 1046–1050.
- B. S. Broyles, S. C. Jacobson and J. M. Ramsey, *Anal. Chem.*, 2003, **75**, 2761–2767.
- C. Yu, M. H. Davey, F. Svec and J. M. J. Frechet, *Anal. Chem.*, 2001, **73**, 5088–5096.
- K. G. Olsen, D. J. Ross and M. J. Tarlov, *Anal. Chem.*, 2002, **74**, 1436–1441.
- R. D. Oleschuk, L. L. Shultz-Lockyear, Y. Ning and D. J. Harrison, *Anal. Chem.*, 2000, **72**, 585–590.
- P. Gebauer and P. Bocek, *Electrophoresis*, 2000, **21**, 3898–3904.
- P. A. Walker, III, M. D. Morris, M. A. Burns and B. N. Johnson, *Anal. Chem.*, 1998, **70**, 3766–3769.
- J. L. Beckers and F. M. Everaerts, *J. Chromatogr.*, 1990, **508**, 3–17.
- Y. Sera, N. Matsubara, K. Otsuka and S. Terabe, *Electrophoresis*, 2001, **22**, 3509–3513.
- J. P. Quirino and S. Terabe, *Anal. Chem.*, 1999, **71**, 1638–1644.
- P. G. Righetti and A. Bossi, *Anal. Chim. Acta*, 1998, **372**, 1–19.
- D. Ross and L. E. Locascio, *Anal. Chem.*, 2002, **74**, 2556–2564.
- J. Han and H. G. Craighead, *Science*, 2000, **288**, 1026–1029.
- G. M. Walker and D. J. Beebe, *Lab Chip*, 2002, **2**, 57–61.
- E. B. Cummings, S. K. Griffiths, R. H. Nilson and P. H. Paul, *Anal. Chem.*, 2000, **72**, 2526–2532.
- C. Khoury, T. Adalsteinsson, B. Johnson, W. C. Crone and D. J. Beebe, *Biomed. Microdevices*, 2003, **5**, 35–45.
- S. K. De, N. R. Aluru, B. Johnson, W. C. Crone, D. J. Beebe and J. S. Moore, *J. Microelectromech. Syst.*, 2002, **11**, 544–555.
- D. J. Beebe, J. S. Moore, J. M. Bauer, Q. Yu, R. H. Liu, C. Devadoss and B.-H. Jo, *Nature*, 2000, **404**, 588–590.
- G. H. Seong, W. Zhan and R. M. Crooks, *Anal. Chem.*, 2002, **74**, 3372–3377.
- J. Heo, K. J. Thomas, G. H. Seong and R. M. Crooks, *Anal. Chem.*, 2003, **75**, 22–26.
- R. A. Zangmeister and M. J. Tarlov, *Anal. Chem.*, 2004, **76**, 3655–3659.
- R. A. Zangmeister and M. J. Tarlov, *Langmuir*, 2003, **19**, 6901–6904.
- J. C. McDonald, D. C. Duffy, J. R. Anderson, D. T. Chiu, W. Hongkai, O. J. A. Schueller and G. M. Whitesides, *Electrophoresis*, 2000, **21**, 27–40.
- A. Revzin, R. J. Russell, V. K. Yadavalli, W.-G. Koh, C. Deister, D. D. Hile, M. B. Mellott and M. V. Pishko, *Langmuir*, 2001, **17**, 5440–5447.
- T. Canal and N. A. Peppas, *J. Biomed. Mater. Res.*, 1989, **23**, 1183–1193.
- J. J. Nakane, M. Akeson and A. Marziali, *J. Phys.: Condens. Matter*, 2003, **15**, R1365–R1393.
- S. M. Bezrukov, *J. Membr. Biol.*, 2000, **174**, 1–13.
- The size of fluorescein was calculated using the known bond length data: see, for example, *Handbook of Chemistry and Physics*, 70th edn., eds. R. C. Weast *et al.*, CRC Press, Boca Raton, FL, 1989.
- See ESI.
- O. H. Griffith, W. A. Houle, K. F. Kongsli and W. W. Sukow, *Ultramicroscopy*, 1984, **12**, 299–308.
- T.-C. Kuo, D. M. J. Cannon, Y. Chen, J. J. Tulock, M. A. Shannon, J. V. Sweedler and P. W. Bohn, *Anal. Chem.*, 2003, **75**, 1861–1867.
- D. M. J. Cannon, T.-C. Kuo, P. W. Bohn and J. V. Sweedler, *Anal. Chem.*, 2003, **75**, 2224–2230.
- A. J. Bard and L. R. Faulkner, *Electrochemical Methods, Fundamentals and Applications*, Wiley, New York, 1980.
- C. L. Rice and R. Whitehead, *J. Phys. Chem.*, 1965, **69**, 4017–4024.
- A. S. Rathore and A. Guttman, *Electrokinetic Phenomena*, Marcel Dekker, Inc., New York, 2004.